Journal of Power Sources 269 (2014) 949–961

Contents lists available at ScienceDirect

Journal of Power Sources

journal homepage: www.elsevier.com/locate/jpowsour

A robust approach to battery fuel gauging, part II: Real time capacity estimation

B. Balasingam*, G.V. Avvari, B. Pattipati, K.R. Pattipati, Y. Bar-Shalom

Department of Electrical and Computer Engineering, University of Connecticut, 371 Fairfield Way, U-2157, Storrs, CT 06269 USA

HIGHLIGHTS

- Online, adaptive RLS and TLS estimates of battery capacity are derived in closed form.
- The derivations include exact weights and covariance matrices that improve accuracy.
- A second method of capacity estimation is demonstrated by exploiting battery rests.
- An optimal fusion algorithm combines independent estimates of capacity for robustness.

ARTICLE INFO

Article history:
Received 17 January 2014
Received in revised form
17 June 2014
Accepted 1 July 2014
Available online 17 July 2014

Keywords:
Battery management system (BMS)
Battery fuel gauge (BFG)
Li-ion battery
Capacity estimation
Capacity fade

ABSTRACT

In this paper, the second of a series on battery fuel gauging, we present an approach for real time capacity estimation. In part I of this series, we presented a real time parameter estimation approach for various battery equivalent models. The proposed capacity estimation scheme has the following novel features: it employes total least squares (TLS) estimation in order to account for uncertainties in both model and the observations in capacity estimation. The TLS method can adaptively track changes in battery capacity. We propose a second approach to estimate battery capacity by exploiting rest states in the battery. This approach is devised to minimize the effect of hysteresis in capacity estimation. Finally, we propose a novel approach for optimally fusing capacity estimates obtained through different methods. Then, the proposed algorithm was validated using hardware-in-the-loop (HIL) data collected from commercially available Li-ion batteries. The proposed approach performs within 1% or better accuracy in terms of capacity estimation based on both simulated as well as HIL evaluations.

1. Introduction

The state of charge (SOC) of the battery, defined as.

$$\text{SOC} = \frac{\text{Remaining charge in Ampere hours (Ah)}}{\text{Capacity of the battery in Ampere hours (Ah)}} \quad (1)$$

provides vital information about the status of the battery. Numerous approaches can be found in the literature for tracking the SOC of the battery. The knowledge of SOC and battery capacity are used to estimate the time to shut down (TTS) or time to fully charge (TTF) the battery. It is understood that the battery capacity varies with temperature and that it fades over time depending on usage patterns and age. Accurate tracking of battery capacity is a critical element of battery fuel gauging; however, it has received relatively little attention in the literature.

Some important contributions to battery capacity estimation were presented in Refs. [1–3]. In Ref. [1] a method of estimating battery capacity based on SOC lookup of a resting battery and the amount of transferred charge was reported. This method neglects the hysteresis effect [4] and assumes that the rested battery voltage represents the true open circuit voltage (OCV) of the battery. Further, the proposed approach in Ref. [4] is not designed to track capacity drifts over time. In Ref. [3] a weighted total least square (TLS) estimation scheme was proposed for online battery capacity estimation. The exact value of the weights were not derived in Ref. [3] and the developed TLS method was not directly extendable to adaptive estimation. In Ref. [2], a data driven approach for

* Corresponding author.
E-mail addresses: bala@engr.uconn.edu (B. Balasingam), vinod@engr.uconn.edu (G.V. Avvari), bharath@engr.uconn.edu (B. Pattipati), krishna@engr.uconn.edu (K.R. Pattipati), ybs@engr.uconn.edu (Y. Bar-Shalom).

http://dx.doi.org/10.1016/j.jpowsour.2014.07.032
0378-7753/

List of notations

C_{batt}	capacity of the battery, (2)
c_h	coulomb counting coefficient, (6)
$\widehat{C}_{\text{LS}}$	LS estimate of battery capacity, (22)
$\widehat{C}_{\text{RLS}}$	RLS estimate of battery capacity, (25)
$\widehat{C}_{\text{TLS}}$	TLS estimate of the battery capacity, (29)
$\mathbf{d}_c^{\kappa}$	vector of SOC differences, (16)
$\mathbf{d}_{c,\text{ocv}}^{\kappa}$	vector of SOC differences between two rests, (45)
$\mathbf{d}_s^{\kappa}$	vector of Coulombs, (16)
$\mathbf{d}_{s,\text{ocv}}^{\kappa}$	vector of Coulombs between two rests, (45)
$\mathbf{H}^{\kappa}$	augmented observation matrix, (26)
$i[k]$	current through the battery, (3)
K_i	OCV parameters: K_0, K_1, K_2, K_3, K_4, K_5, K_6, K_7, (33)
$n_i[k]$	noise in measured current, (3)
$P_s[k\|k]$	SOC estimation error variance, (15)
$Q_c[\kappa]$	variance of capacity drift, (51)
$R_c[\kappa]$	capacity estimation error by TLS, RLS or OCV method, (52)
$\widehat{R}_{\text{RLS}}[\kappa]$	RLS capacity estimation error variance, (23)
$R_{\text{TLS}}[\kappa]$	TLS capacity estimation error variance, (31)
$w_s[k]$	process noise, (4)
$\tilde{w}_s[k]$	differential SOC error, (12)
$\overline{w}_s^k$	accumulative of process noise between rest at k and the subsequent rest, (40)
$\tilde{w}_{s,\text{ocv}}^k$	differential SOC error based on OCV lookup, (44)
$\tilde{\mathbf{w}}_s^{\kappa}$	vector of differential SOC errors, (16)
$\tilde{\mathbf{w}}_{s,\text{ocv}}^{\kappa}$	vector of differential OCV based SOC errors, (45)
$x_c[\kappa]$	fused battery capacity, (51)
$\widehat{x}_s[k\|k]$	SOC estimate, (8)
$x_s[k+1]$	SOC, (2)
$\widehat{x}_{s,\text{ocv}}[k]$	OCV lookup based SOC estimate, (35)
$\tilde{x}_{s,\text{ocv}}[k]$	error in OCV lookup based SOC estimate, (36)
$z_c[\kappa]$	capacity estimates by TLS, RLS or OCV method, (52)
$z_i[k]$	measured current, (3)
$\boldsymbol{\epsilon}_{C_{\text{batt}}}[k]$	capacity estimation error, (58)
η_c	charging efficiency ($\eta = \eta_c$), (7)
η_d	discharging efficiency ($\eta = \eta_d$), (7)
$\mathbf{S}_{\mathbf{H}}^{\kappa}$	covariance of the augmented observation matrix, (27)
$\boldsymbol{\Sigma}_{\tilde{\mathbf{w}}_s}^{\kappa}$	covariance of differential SOC errors, (20)

concurrent estimation of SOC, parameters an battery capacity is presented.

In this paper, we address the drawbacks of the existing approaches to online capacity estimation and develop an approach with the following novel features:

- *A weighted recursive least squares (RLS) estimate of capacity with the derivation of the exact weights.* Similarly to [3], we derive a weighted RLS approach for online capacity estimation. However, we also derive exact expressions for the weights based on the variances and covariances across times of the updated SOC tracking and the current measurement error standard deviation.
- *A novel TLS approach for real time tracking of battery capacity.* We develop a novel TLS approach that gives a closed form expression for capacity estimation. This approach can be used for continuously tracking changes in the battery capacity.
- *A novel method for adaptive capacity estimation based on OCV lookup of a rested battery.* We develop a TLS approach for online tracking of battery capacity by exploiting battery resting instances for OCV lookup based SOC estimation.
- *A robust approach for optimal fusion of capacity estimates obtained through different approaches.* We develop a robust approach for optimally and adaptively fusing capacity estimates obtained through two different approaches.

In Ref. [5], part I of this series, we presented an approach for real time parameter estimation for various battery equivalent models, and in Ref. [6], part III of this series, we develop an SOC tracking approach, assuming the knowledge of parameter and capacity estimates. Fig. 1 shows a block diagram of the BFG and the steps followed to obtain it. We briefly describe each of the blocks below.

- *Offline data collection.* The understanding of the behaviors of a battery is achieved through a combination of physical,

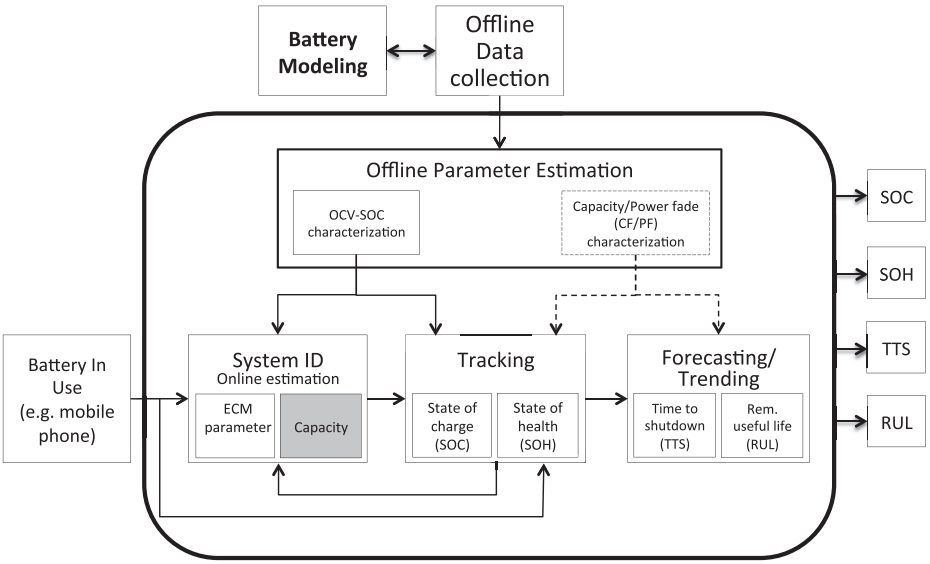

Fig. 1. Elements of a BFG. The focus of the present paper, capacity estimation, is shaded in grey. The dashed lines indicate that the CF/PF models are not used in tracking SOH and computing RUL in the present paper series.

electrochemical model based explanations and through data. For example, a particular battery cell having a certain maximum voltage and the fact that there exists a monotonic relationship between the OCV and SOC of the battery can be explained based on electrochemical understanding; the modeling of OCV-SOC relationship as a *Combined+2* model [7] is achieved through data. As far as the BFG algorithm development is concerned, the data collection plays an important part in understanding different models, such as, OCV-SOC, CF and PF models, that are required for accurate fuel gauging. It must be noted that data collection and battery modeling go hand in hand until adequate models are defined and the parameters estimated.

- *Battery modeling.* There are different paradigms in batter modeling as it applies to fuel gauging, such as electrical equivalent circuit models (ECM) based approaches [5,6,8], electrochemical modeling based approaches [9] and data driven approaches [10–12]. Our BFG approach is based on ECM, hence, our discussions and descriptions are related to ECM modeling based BFGs where the following five aspects of the battery behavior are studied and models developed.
  1. *OCV.* The characteristics of OCV-SOC relationship were extensively studied in the literature (see Ref. [7] and the references therein). It is understood that the OCV-SOC relationship is stable over temperature changes and aging. It must be noted that even though there exists a clearly understood OCV-SOC characteristic for which the parameters can be accurately estimated, the SOC cannot be simply computed based on the measured voltage; the *dynamic behavior of the battery* has to be accounted for before computing SOC based on measured voltage.
  2. *Battery capacity.* Battery capacity denotes the total amount of Coulombs that can be discharged from the battery. Battery capacity is a key battery parameter in computing the state of charge online, through *Coulomb counting.*
  3. *Dynamic behavior of the battery.* The measured terminal voltage of the battery is not always equal to the OCV. The *voltage drop* between the OCV and the battery terminal is modeled through ECM (also see Fig. 4).
  4. *Capacity fade (CF).* Battery capacity is known to degrade as a result of aging, temperature and DoD (frequent DoD values closer to both 0 and 1 negatively affect capacity [13]). Unlike OCV modeling, which requires data from just one charge–discharge cycle, CF modeling requires extensive data, over several hundreds of cycles, for analysis; the CF modeling requires continuous data from new-to-dead battery under various temperature, aging and DoD scenarios.
  5. *Power fade (PF).* Similar to CF, the ECM parameters change as a result of temperature, aging and depth of discharge (DoD) patterns a battery undergoes. Especially, the internal resistances increase as a result of aging and this limits the amount of power that can be drawn from the battery; resulting in *power fade.* In addition, it must be noted that the available power varies instantaneously as a result of temperature changes and this adds an extra layer of difficulty in modeling.
- Offline parameter estimation.
  - *OCV model parameters.* For OCV parameter estimation, slow discharge data is required for an entire discharge–charge cycle. Several models, such as linear, polynomial, exponential and combinations of these have been proposed in the literature. We present a summary of the existing OCV modeling approaches in Ref. [7].
  - *CF parameters.* There has been significant interest in developing a capacity fade model. Several data analyses and attempts at creating a CF model can be found in Refs. [13–21].
  - *PF parameters.* Some examples of PF modeling and parameter estimation are found in Refs. [22–25].
- *Online parameter estimation (system ID).* Given the OCV parameters of the battery, the ECM parameters and the battery capacity can be estimated online. Indeed, there are some recent works [2,26,27] that attempt to estimate the OCV parameters online as well.
  - *OCV.* In this paper we assume the knowledge of offline estimated OCV parameters that are used in the estimation of capacity and ECM parameters. In Refs. [2,26,27], some approaches are developed to estimate the OCV parameters online.
  - *Capacity.* The focus of the present paper is online capacity estimation. We develop two different approaches for online capacity estimation and present an optimal fusion technique that results in a robust strategy for battery capacity estimation.
  - *ECM parameters.* We develop a novel strategy for the estimation of ECM parameters in Ref. [5]; the developed approach is significantly novel compared to the existing approaches.
- Tracking.
  - *SOC.* A clear understanding of the OCV-SOC models led to the development of SOC tracking as a recursive Bayesian estimation problem that can be solved through non-linear filters such as extended Kalman filter. The Coulomb counting model represents the instantaneous changes in SOC and serves as the process (plant) model; the OCV + ECM model establishes a relationship between the measured voltage and SOC, serving as the observation model for SOC tracking.
  - *SOH (PF and CF).* Unlike SOC, the SOH changes slowly, hence, there is no need to track the SOH at the same frequency as SOC. Several models developed in Refs. [13–21] present CF and PF in terms of the number of cycles. Unlike OCV-SOC relationship, the CF/PF-cycle relationship is much more complicated; the cycle cannot be uniquely defined; the effects of temperature exposure, depth of discharge (DoD) significantly affect the model; the patterns of temperature exposure and DoD are not uniquely defined. Hence, online estimated capacity and ECM parameter values are well suited

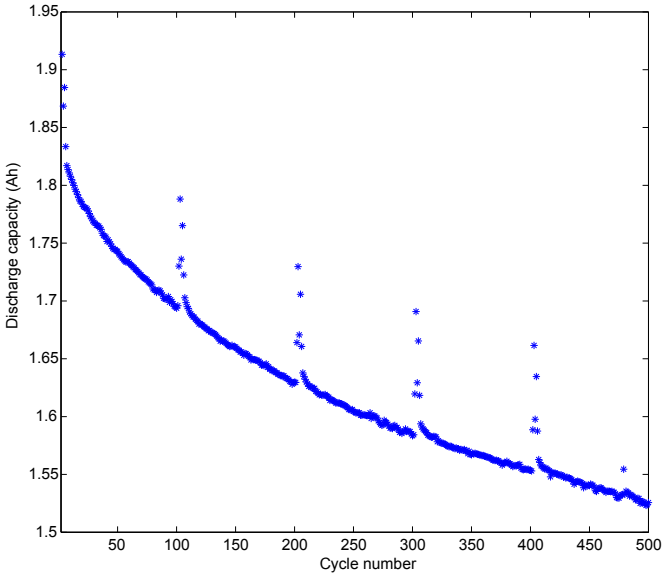

Fig. 2. Discharge capacity over 500 cycles. The battery is discharged at 1.5 A rate. Slower discharge rates are used for ten consecutive cycles in every 100 cycles.

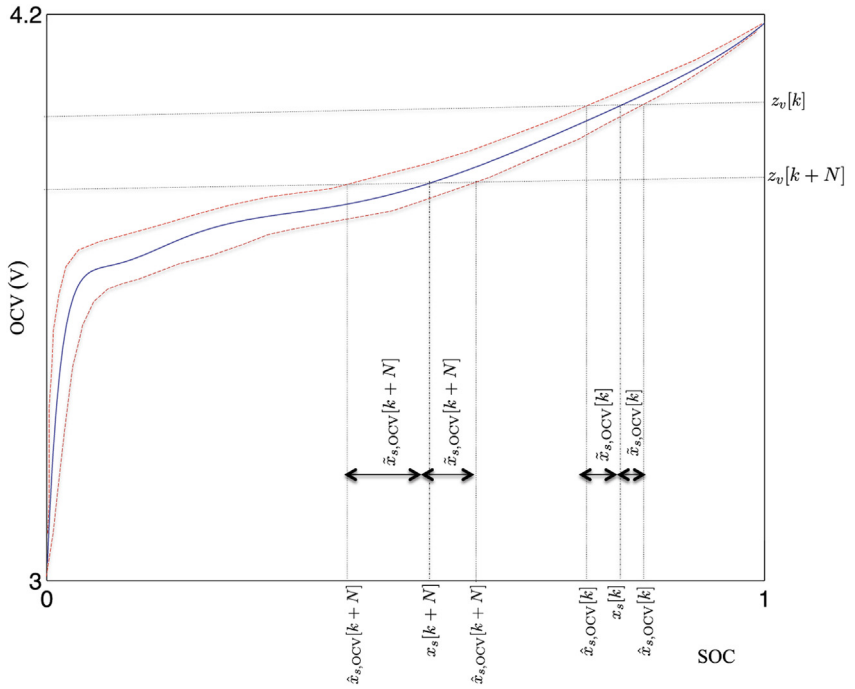

Fig. 3. Generic description of OCV lookup based SOC estimates and the OCV lookup error. The solid line in blue shows the true OCV-SOC characteristics. The dashed lines in red describe the effect of hysteresis when the battery comes to rest after charging or discharging: The dashed line in red above the true OCV-SOC curve (solid line) corresponds to hysteresis after charging and the dashed line in red below the true OCV-SOC curve (solid line) corresponds to hysteresis after discharging. For a given rested voltage $z_v[k]$, the corresponding SOC estimate $\hat{x}_{s,\mathrm{ocv}}[k]$ can be obtained by inverting (33). Due to hysteresis in the battery, this SOC estimate $\hat{x}_{s,\mathrm{ocv}}[k]$ will differ from the actual SOC $x_s[k]$, resulting in an OCV lookup error $\tilde{x}_{s,\mathrm{ocv}}[k]$. The OCV lookup error will always be negative during discharging and positive during charging.(For interpretation of the references to colour in this figure legend, the reader is referred to the web version of this article.)

for battery fuel gauging. It must be noted that the online estimated capacity and ECM parameters can be improved with the help of CF/PF models, which is beyond the scope of this paper.

- Forecasting/Trending.
  - *TTS.* In practical battery applications, the batteries are fitted with protective circuitry that switch off the device once a particular shut down voltage is reached. Predicting TTS requires the knowledge of the ECM parameters; usually the TTS prediction is made for a particular load, e.g., TTS for voice, TTS for video etc.
  - *RUL.* Similar to TTS, the RUL predicts the remaining cycles until a certain SOH is reached.

It must be noted that, each estimation/tracking/forecasting block (module) in Fig. 1 must be performed at different time scales.

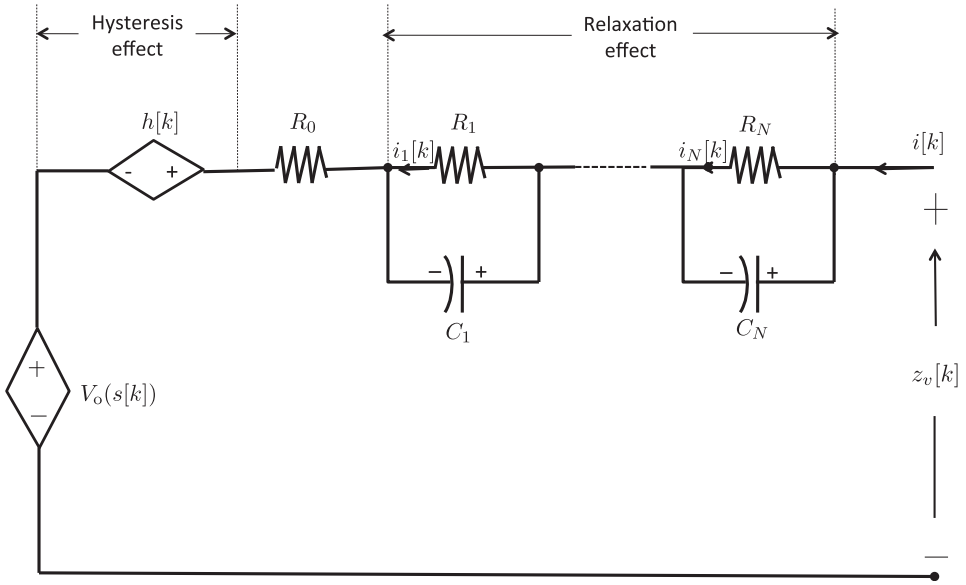

Fig. 4. Equivalent circuit model (ECM) of the battery. The open circuit voltage (OCV) is denoted by Refs. $V_o(s[k])$, $h[k]$ denotes the hysteresis of the battery at time k, and $i_N[k]$ denotes the current through the resistor R_N. The relaxation effect becomes zero (voltage) when the battery is rested whereas the hysteresis effect remains unaffected by resting the battery.

In Table 1, we describe the time scales at which each of these modules operate.

It is important to distinguish the online capacity estimation method presented in this paper (and also in Refs. [1] and [3]) against any CF models that can also be used to estimate battery capacity at a given cycle. For an example of CF models, let us refer to Fig. 2, which shows the discharge capacity of a Li-ion battery over 500 cycles. A simple CF model can be obtained by fitting the discharge capacity vs. cycle data as an exponential decay. Now, given the cycle number, the above CF model can be used for determining the capacity of the battery. The discharge experiment whose results are described in Fig. 2 was conducted over a 60 day period during which the battery experienced the same temperature and charge/discharge patterns. The suitability of the above model in individual battery usage situations cannot be guaranteed. An online capacity estimation method (such as the one developed in this paper) does not depend on CF models, hence, it is applicable to any battery usage conditions.

The rest of the paper is organized as follows. Our procedure for capacity estimation is summarized in Section 2. The performance of the proposed approach is demonstrated through experimental results in Section 3, and the paper is concluded in Section 4.

2. Battery capacity estimation and fusion

The instantaneous state of charge (SOC) of the battery can be written as the following process model, which is also known as the Coulomb counting equation, in terms of the measured current as follows:

$$x_s\left[k+1\right] = x_s\left[k\right] + \frac{\eta\Delta}{3600C_{\text{batt}}} z_i\left[k\right] + w_s\left[k\right] \tag{2}$$

where $x_s[k] \in [0,1]$ denotes the SOC of the battery, C_{batt} is the capacity of the battery in Ampere hours (Ah) and $z_i[k]$ is the measured current

$$z_i[k] = i[k] + n_i[k] \tag{3}$$

which is corrupted by zero mean white noise $n_i[k]$ with standard deviation (s.d.) σ_i.

The process noise in (2) relates to the measurement noise in (3) as.

$$w_s[k] = -c_h \Delta n_i[k] \tag{4}$$

and is zero mean with s.d.

Table 1
Time scales of various state and parameter estimation in BFG.

	Offline	Tiny scale (milliseconds)	Small scale (seconds/minutes)	Medium scale (hours)	Large scale (cycles/days)
Offline parameter estimation	OCV(SOC), CF(DoD, temperature, other), PF(DoD, temperature, other)				
Online parameter estimation			ECM parameters	Capacity	
Tracking		SOC		SOH (PF and CF)	
Trending (forecasting)		TTS			RUL

$$\sigma_s = c_h \Delta \sigma_i \tag{5}$$

where the Coulomb counting coefficient is

$$c_h \triangleq \frac{\eta}{3600C_{\text{batt}}} \tag{6}$$

Here, η is a constant that depends on whether the battery is being charged or discharged, i.e.,

$$\eta = \begin{cases} \eta_c & i[k] > 0 \\ \eta_d & i[k] < 0 \end{cases} \tag{7}$$

and Δ is the (constant) sampling interval.

2.1. BFG-based online battery capacity estimation using RLS

In Ref. [6], we discuss ways to estimate the SOC based on both voltage and current measurements. Two consecutive SOC values $x_s[k]$ and $x_s[k+1]$ are written in terms of their estimates as.

$$x_s[k] = \hat{x}_s[k|k] + \tilde{x}_s[k|k] \tag{8}$$

$$x_s[k+1] = \hat{x}_s[k+1|k+1] + \tilde{x}_s[k+1|k+1] \tag{9}$$

where the estimation errors $\tilde{x}_s[k|k]$ and $\tilde{x}_s[k+1|k+1]$ have zero mean and variances $P_s[k|k]$ and $P_s[k+1|k+1]$, respectively. The covariance between two consecutive estimation errors is [[28], problem 5–10]

$$E\{\tilde{x}_s[k|k]\tilde{x}_s[k+1|k+1]\} = (1 - G[k+1]H[k+1])P_s[k|k] \tag{10}$$

where $G[k+1]$ is the scalar Kalman gain and $H[k+1]$ is the scalar linearized observation model at time $k+1$. The details about $G[k+1]$ and $H[k+1]$ can be found in Ref. [6].

Now, let us rewrite (2) in the following form.

$$x_s\left[k+1\right] - x_s\left[k\right] = \frac{\eta\Delta}{3600C_{\text{batt}}} z_i\left[k\right] + w_s\left[k\right] \tag{11}$$

Substituting (8) and (9) in (11) yields.

$$\Delta x_s\left[k+1,k\right] \triangleq \hat{x}_s\left[k+1\middle|k+1\right] - \hat{x}_s\left[k\middle|k\right] = \frac{\eta_h\Delta}{C_{\text{batt}}} z_i\left[k\right] + \tilde{w}_s\left[k\right] \tag{12}$$

where

$$\eta_h = \frac{\eta}{3600} \tag{13}$$

and the differential error given by

$$\tilde{w}_s[k] = \tilde{x}_s[k|k] - \tilde{x}_s[k+1|k+1] + w_s[k] \tag{14}$$

is zero mean with variance (see proof in Appendix A)

$$E\left\{\tilde{w}_s[k]^2\right\} \triangleq R_{\tilde{w}_s[k]} = G[k+1]^2 S\left[k+1\right] \tag{15}$$

where $S[k+1]$ is the innovation covariance of the Kalman filter (The details about the Kalman filter for SOC tracking can be found in Ref. [6]).

By considering a batch of L_c of samples, (12) can be written in vector from as follows.

$$\mathbf{d}_s^{\kappa} = C_{\text{batt}}^{-1}\mathbf{d}_c^{\kappa} + \tilde{\mathbf{w}}_s^{\kappa} \tag{16}$$

where κ is the batch number, L_c is the length of the batch,

$$\mathbf{d}_s^{\kappa} = [\Delta x_s[\kappa L_c - L_c + 1, \kappa L_c - L_c] \quad \Delta x_s[\kappa L_c - L_c + 2, \kappa L_c - L_c + 1 \ldots \Delta x_s[\kappa L_c, \kappa L_c - 1]]^T$$

$$\mathbf{d}_c^{\kappa} = [\eta_h \Delta_{\kappa L_c - L_c + 1} z_i[\kappa L_c - L_c + 1] \quad \eta_h \Delta_{\kappa L_c - L_c + 1} z_i[\kappa L_c - L_c + 2] \ldots \eta_h \Delta_{\kappa L_c} z_i[\kappa L_c]]^T$$

$$\tilde{\mathbf{w}}_s^{\kappa} = [\tilde{w}[\kappa L_c - L_c + 1] \quad \tilde{w}[\kappa L_c - L_c + 2] \ldots \tilde{w}[\kappa L_c]]^T \tag{19}$$

and $\tilde{\mathbf{w}}_s^{\kappa}$ is a white Gaussian noise vector with covariance

$$\mathbf{\Sigma}_{\tilde{\mathbf{w}}_s}^{\kappa} = E\left\{\tilde{\mathbf{w}}_s^{\kappa}(\tilde{\mathbf{w}}_s^{\kappa})^T\right\} \tag{20}$$

which is an $L_c \times L_c$ diagonal matrix with its nth diagonal element given by

$$\left(\mathbf{\Sigma}_{\tilde{\mathbf{w}}_s}^{\kappa}\right)_{nn} = G[\kappa L_c - L_c + n]^2 S\left[\kappa L_c - L_c + n\right] \tag{21}$$

Now, the LS estimate[1] of the inverse battery capacity is given by.

$$\widehat{C}_{\mathrm{LS}}^{-1} = \left((\mathbf{d}_c^{\kappa})^T \left(\mathbf{\Sigma}_{\tilde{\mathbf{w}}_s}^{\kappa}\right)^{-1} \mathbf{d}_c^{\kappa}\right)^{-1} (\mathbf{d}_c^{\kappa})^T \left(\mathbf{\Sigma}_{\tilde{\mathbf{w}}_s}^{\kappa}\right)^{-1} \mathbf{d}_s^{\kappa} \tag{22}$$

and the variance of the LS inverse capacity estimate is

$$\widehat{R}_{\mathrm{RLS}}[\kappa] = \left((\mathbf{d}_c^{\kappa})^T \left(\mathbf{\Sigma}_{\tilde{\mathbf{w}}_s}^{\kappa}\right)^{-1} \mathbf{d}_c^{\kappa}\right)^{-1} \tag{23}$$

When a new batch of $\{\mathbf{d}_s^{\kappa+1}, \mathbf{d}_c^{\kappa+1}\}$ pair arrives, the LS estimates can be recursively updated by.

$$\widehat{R}_{\mathrm{RLS}}^{-1}\left[\kappa + 1\right] = \lambda \widehat{R}_{\mathrm{RLS}}^{-1}\left[\kappa\right] + \left(\mathbf{d}_c^{\kappa+1}\right)^T \left(\mathbf{\Sigma}_{\tilde{\mathbf{w}}_s}^{\kappa+1}\right)^{-1} \mathbf{d}_c^{\kappa+1} \tag{24}$$

$$\widehat{C}_{\mathrm{RLS}}^{-1}\left[\kappa + 1\right] = \widehat{R}_{\mathrm{RLS}}\left[\kappa + 1\right]\left(\lambda \widehat{R}_{\mathrm{RLS}}^{-1}\left[\kappa\right] \widehat{C}_{\mathrm{RLS}}^{-1}\left[\kappa\right] + \left(\mathbf{d}_c^{\kappa+1}\right)^T \left(\mathbf{\Sigma}_{\tilde{\mathbf{w}}_s}^{\kappa+1}\right)^{-1} \mathbf{d}_b^{\kappa+1}\right) \tag{25}$$

where $\widehat{R}_{\mathrm{RLS}}^{-1}[\kappa]$ is the $L_c \times L_c$ information matrix for capacity estimation and λ is the fading memory constant.

It must be noted that $\mathbf{d}_c^{\kappa}$ in (16) is constructed from measured current values that are known to be noisy whereas the LS and RLS estimation methods discussed earlier assume that $\mathbf{d}_c^{\kappa}$ is perfectly known. For a more realistic solution, one should consider the uncertainty in $\mathbf{d}_c^{\kappa}$. Next, we propose an approach based on total least squares (TLS) optimization that addresses errors in $\mathbf{d}_c^{\kappa}$.

2.2. BFG-based online battery capacity estimation using adaptive TLS

In this section, we develop an online capacity estimation method based on TLS which assumes uncertainty in both $\mathbf{d}_s^{\kappa}$ and $\mathbf{d}_c^{\kappa}$ in (16). For more details about the TLS method, the reader is referred to [29] and the references therein.

Let us construct the following augmented observation matrix.

$$\mathbf{H}^{\kappa} = \left[\mathbf{d}_s^{\kappa} \quad \mathbf{d}_c^{\kappa}\right] \tag{26}$$

The information matrix associated with the augmented observation matrix is.

$$\mathbf{S}_{\mathbf{H}}^{\kappa} = (\mathbf{H}^{\kappa})^T \mathbf{H}^{\kappa} \tag{27}$$

Let us write the eigendecomposition of $\mathbf{S}_{\mathbf{H}}^{\kappa}$ in the following form.

$$\mathbf{S}_{\mathbf{H}}^{\kappa} = \mathbf{V}^{\kappa} \mathbf{\Lambda}^{\kappa} \mathbf{V}^{\kappa T} \tag{28}$$

where

- $\mathbf{\Lambda}^{\kappa}$ is a diagonal 2×2 matrix of nonnegative eigenvalues arranged from the largest to the smallest, i.e., $\mathbf{\Lambda}^{\kappa}(1,1)$ denotes the largest eigen value and $\Lambda^{\kappa}(2,2)$ denotes the smallest eigenvalue.
- Each column of the 2×2 matrix $\mathbf{V}^{k} = [\mathbf{v}_1^{\kappa}, \mathbf{v}_2^{\kappa}]$ has the corresponding eigenvectors, i.e., the first column $\mathbf{v}_1^{\kappa}$ is the eigenvector corresponding to the largest eigenvalue and the second column $\mathbf{v}_2^{\kappa}$ is the eigenvector corresponding to the smallest eigenvalue.

The TLS estimate of the inverse battery capacity is then given by the ratio of the components of $\mathbf{v}_2^{\kappa}$, namely.

$$\widehat{C}_{\mathrm{TLS}}^{-1}\left[\kappa\right] = -\frac{\mathbf{v}_2^{\kappa}(1)}{\mathbf{v}_2^{\kappa}(2)} = \frac{\mathbf{S}_{\mathbf{H}}^{\kappa}(1,2)}{\mathbf{S}_{\mathbf{H}}^{\kappa}(1,1) - \mathbf{\Lambda}^{\kappa}(2,2)} \tag{29}$$

where $\mathbf{v}_2^{\kappa}(i)$ is the i^{th} element of $\mathbf{v}_2^{\kappa}$ and $\mathbf{S}_{\mathbf{H}}^{\kappa}(i,j)$ is the $(i,j)^{\mathrm{th}}$ element of $\mathbf{S}_{\mathbf{H}}^{\kappa}$. The derivation of (29) is shown in Appendix B.

For smoother estimates, the information matrix in (27) can be updated with a fading memory, as follows

$$\mathbf{S}_{\mathbf{H}}^{\kappa} = \lambda \mathbf{S}_{\mathbf{H}}^{\kappa-1} + \frac{(\mathbf{H}^{\kappa})^T \mathbf{H}^{\kappa}}{L_c - 1} \tag{30}$$

Now, based on [30], the TLS estimation error covariance is (approximately)

$$\widehat{R}_{\mathrm{TLS}}[\kappa] = \left(\frac{1}{(\mathbf{z}^{\kappa})^T \mathbf{S}_{\mathbf{H}}^{\kappa} \mathbf{z}^{\kappa}} \sum_{i=1}^{M} \mathbf{h}_i^{\kappa} (\mathbf{h}_i^{\kappa})^T\right)^{-1} \tag{31}$$

where $\mathbf{h}_i^{\kappa}$ is the i^{th} row of $\mathbf{H}^{\kappa}$, M is the number of rows in $\mathbf{H}^{\kappa}$ and

$$\mathbf{z}^{\kappa} = \begin{bmatrix} -\frac{\mathbf{v}_2^{\kappa}(1)}{\mathbf{v}_2^{\kappa}(2)} & -1 \end{bmatrix}^T \tag{32}$$

2.3. OCV-based online battery capacity estimation

The open circuit voltage (OCV) of the battery can be written as a nonlinear function of SOC as.

$$V_0(x_s[k]) = K_0 + \frac{K_1}{x_s[k]} + \frac{K_2}{x_s[k]^2} + \frac{K_3}{x_s[k]^3} + \frac{K_4}{x_s[k]^4} + K_5 x_s[k] + K_6 \ln(x_s[k]) + K_7 \ln(1 - x_s[k]) \tag{33}$$

where the coefficients K_0, K_1, K_2, K_3, K_4, K_5, K_6 and K_7 can be estimated offline by collecting voltage and current measurements by slowly charging and then discharging the battery (see Ref. [7]). A typical OCV-SOC characterization curve is shown in Fig. 3 in blue.

To illustrate this further, consider the equivalent circuit model (ECM) of the battery, shown in Fig. 4.[2] The OCV, which is a function

[1] This is an approximate LS estimate because both (17) and (18) are noisy. An algorithm based on TLS is described in the next subsection.

[2] This numbering is again specific to this document.

of SOC, is denoted by $V_\circ(s[k])$ where $s[k]$ is the SOC at time k. The relaxation effect of the battery is modeled as a series of *RC* circuits; when the battery is fully at rest the relaxation effect become zero, i.e., when there is no current activity through the battery for sufficient time, the voltage across the *RC* circuits becomes zero. "*The hysteresis in Li-ion batteries is generated due to the thermodynamic entropic effects, mechanical stress, and microscopic distortions within the active electrode materials during Lithium insertion/extraction* [4]". The hysteresis effect does not vanish when resting the battery. When the battery is fully rested, the measured voltage can be written as

$$z_v[k] = V_\circ(s[k]) + h[k] \tag{34}$$

where the hysteresis $h[k]$ corrupts the measured OCV.

The OCV-SOC characteristic curve can be used to get a measure of SOC whenever the battery is sufficiently rested. The SOC of the battery for a given at-rest terminal voltage (which is also the open circuit voltage) $z_v[k]$, written as

$$\widehat{x}_{s,\mathrm{ocv}}\left[k\right] = f^{-1}_{\mathrm{ocv-soc}}(z_v[k]) \tag{35}$$

can be computed using the OCV-SOC characterization by computing the inverse of (33). There are several methods for computing the inverse of a nonlinear function, such as Newton's method and binary search [31]. We also refer to this as *OCV lookup* based SOC estimate.

The SOC estimate in (35) is corrupted by the hysteresis voltage as follows

$$x_s\left[k\right] = \widehat{x}_{s,\mathrm{ocv}}\left[k\right] + \tilde{x}_{s,\mathrm{ocv}}\left[k\right] \tag{36}$$

where the *OCV lookup error* $\tilde{x}_{s,\mathrm{ocv}}[k]$ is caused by the hysteresis effect in OCV (see Fig. 3 also). It must be noted from Fig. 3 that when the battery comes to rest at time k after a discharging process, the OCV lookup error $\tilde{x}_{s,\mathrm{ocv}}[k]$ will always be negative. Similarly, when the battery comes to rest at time k after a charging process, the OCV lookup error $\tilde{x}_{s,\mathrm{ocv}}[k]$ will always be positive. However, the magnitude of the error will vary with the amount of hysteresis, which is a function of the magnitude of the current before rest, SOC and time.

Now, let us rewrite (2) in the following form

$$x_s[k+1] = x_s[k] + c_h\Delta z_i[k] + w_s[k] \tag{37}$$

$$\begin{aligned} x_s[k+2] &= x_s[k+1] + c_h\Delta_{k+1}z_i[k+1] + w_s[k+1] \\ &\vdots \end{aligned} \tag{38}$$

$$x_s[k+N] = x_s[k+N-1] + c_h\Delta_{k+N-1}z_i[k+N-1] + w_s[k+N-1] \tag{39}$$

By adding (37) through (39) on both sides, one arrives at the following:

$$x_s\left[k+N\right] = x_s\left[k\right] + \frac{\eta\sum_{j=k}^{j=K+N-1}\Delta z_i[k]}{3600C_{\mathrm{batt}}} + \underbrace{\sum_{j=k}^{k+N-1} w_s[j]}_{\overline{w}_s^k} \tag{40}$$

where $\overline{w}_s^k$ is zero mean with standard deviation $\sqrt{N}\sigma_s$.

Assuming that the battery is at rest at time k and $k+N$, we can write (40) as.

$$d^k_{s,\mathrm{ocv}} = C^{-1}_{\mathrm{batt}}d^k_{c,\mathrm{ocv}} + \tilde{w}^k_{s,\mathrm{ocv}} \tag{41}$$

where

$$d^k_{c,\mathrm{ocv}} = \frac{\eta\sum_{j=k}^{j=K+N-1}\Delta z_i[k]}{3600} \tag{42}$$

$$d^k_{s,\mathrm{ocv}} = \widehat{x}_{s,\mathrm{ocv}}\left[k+N\right] - \widehat{x}_{s,\mathrm{ocv}}\left[k\right] \tag{43}$$

$$\tilde{w}^k_{s,\mathrm{ocv}} = \underbrace{\tilde{x}_{s,\mathrm{ocv}}\left[k\right] - \tilde{x}_{s,\mathrm{ocv}}\left[k+N\right]}_{\tilde{x}^k_{d,\mathrm{ocv}}} + \overline{w}^k_s \tag{44}$$

It must be noted that, regardless of the fact that the sign of OCV lookup error $\tilde{x}_{s,\mathrm{ocv}}[k]$ is biased towards the battery mode $\in$\{charging,discharging\}, the "differential error" $\tilde{x}^k_{d,\mathrm{ocv}}$ (defined in (44)) can either be positive or negative. By considering a large number of differential errors, we assume $\tilde{x}^k_{d,\mathrm{ocv}}$ is approximately white.

Let us assume that the κ^{th} batch of differential SOCs $\mathbf{d}^\kappa_{s,\mathrm{ocv}}$ is collected between a first set of rest points $k = k_1, k_2,\ldots, k_{Lc}$ and a second set of rest points $k+N = k_1+N_1, k_2+N_2,\ldots, k_{Lc}+N_{Lc}$, respectively, and given by

$$\mathbf{d}^\kappa_{s,\mathrm{ocv}} = C^{-1}_{\mathrm{batt}}\mathbf{d}^\kappa_{c,\mathrm{ocv}} + \tilde{\mathbf{w}}^\kappa_{s,\mathrm{ocv}} \tag{45}$$

where

$$\mathbf{d}^\kappa_{s,\mathrm{ocv}} = \left[d^{k_1}_{s,\mathrm{ocv}},\ d^{k_2}_{s,\mathrm{ocv}},\ \ldots,\ d^{k_{Lc}}_{s,\mathrm{ocv}}\right]^T \tag{46}$$

$$\mathbf{d}^\kappa_{c,\mathrm{ocv}} = \left[d^{k_1}_{c,\mathrm{ocv}},\ d^{k_2}_{c,\mathrm{ocv}},\ \ldots,\ d^{k_{Lc}}_{c,\mathrm{ocv}}\right]^T \tag{47}$$

$$\tilde{\mathbf{w}}^\kappa_{s,\mathrm{ocv}} = \left[w^{k_1}_{s,\mathrm{ocv}},\ w^{k_2}_{s,\mathrm{ocv}},\ \ldots,\ w^{k_{Lc}}_{s,\mathrm{ocv}}\right]^T \tag{48}$$

Now, it can be seen that (45) is in the same form as (16) with $\mathbf{d}^\kappa_{s,\mathrm{ocv}}$, $\mathbf{d}^\kappa_{c,\mathrm{ocv}}$, and $\tilde{\mathbf{w}}^\kappa_{s,\mathrm{ocv}}$ replacing $\mathbf{d}^\kappa_s$, $\mathbf{d}^\kappa_c$, and $\tilde{\mathbf{w}}^\kappa_s$, respectively. Hence, RLS and TLS based capacity estimates can be derived for OCV based observations, by following Sections 2.1 and 2.2 respectively. Let us denote the RLS and TLS estimates of OCV based capacity as $\widehat{C}_{\mathrm{RO}}[\kappa]$ and $\widehat{C}_{\mathrm{TO}}[\kappa]$, respectively.

Remark: It must be noted that, given N_r number of rest states interspersed with a discharge, one can make $N_r(N_r-1)/2$ differential observations. For example, for $N_r = 4$, let us assume the battery is in rest state at time instances t_1, t_2, t_3 and t_4. Table 2 shows the possible rest pairs for differential observations.

In the practical usage of mobile devices, there will be many time epochs of rest state within each cycle of usage. It must be noted that the batch length L_c can be time varying.

2.4. Robust capacity estimation through fusion

In this section, we propose an approach for fusing the TLS estimates of capacity, developed in Section 2.2 and Section 2.3. The TLS approach is found to outperform the RLS approach. Hence, the derivations in this section are developed for TLS based capacity estimate. The exact derivations can be applied for fusing RLS based capacity estimates as well.

The online capacity estimate $\widehat{C}_{\mathrm{TLS}}[\kappa]$ is corrupted by the uncertainty in $\mathbf{d}^\kappa_c$ (see (16)) which is caused by the errors in the measured current and the uncertainty in the $\mathbf{d}^\kappa_s$ which is caused by the errors

in the SOC tracking algorithm. Similarly, the OCV based capacity estimation $\widehat{C}_{\mathrm{TO}}[\kappa]$ is corrupted by the uncertainty in $\mathbf{d}^{\kappa}_{\mathrm{c,ocv}}$ (see (45)) which is caused by the errors in the measured current and the uncertainty in $\mathbf{d}^{\kappa}_{\mathrm{s}}$ that is caused by the OCV lookup differential error. We assume that the errors in online capacity estimates $\mathbf{e}_{\mathrm{t}}[\kappa]$ and the OCV lookup based capacity estimates $\mathbf{e}_{\mathrm{to}}[\kappa]$ are uncorrelated. Based on these assumptions, the capacity the fusion becomes the fusion of two independent tracks [[32], Section 9.2].

First, it must be noted that we estimated the inverse capacities, i.e., the capacity estimates $\widehat{C}^{-1}_{\mathrm{TLS}}[\kappa]$ in (29) and $\widehat{C}^{-1}_{\mathrm{TO}}[\kappa]$ in Sections 2.2, 2.3 respectively are estimates of $1/C_{\mathrm{batt}}$. Correspondingly, the respective estimation error covariances, $\widehat{R}_{\mathrm{TLS}}[\kappa]$ in (31) and $\widehat{R}_{\mathrm{TO}}[\kappa]$ correspond to the inverse capacity estimates as well. Based on Taylor series expansion, the expected value of the TLS based dynamic capacity estimate and the corresponding estimation error variance are approximated as (see Appendix C for details)

$$\widehat{C}_{\mathrm{TLS}}[\kappa] = \frac{1}{\widehat{C}^{-1}_{\mathrm{TLS}}[\kappa]} + \frac{\widehat{R}_{\mathrm{TLS}}[\kappa]}{\left(\widehat{C}^{-1}_{\mathrm{TLS}}[\kappa]\right)^{3}} \tag{49}$$

$$R_{\mathrm{TLS}}[\kappa] = \frac{\widehat{R}_{\mathrm{TLS}}[\kappa]}{\left(\widehat{C}^{-1}_{\mathrm{TLS}}[\kappa]\right)^{4}} \tag{50}$$

where $\widehat{C}_{\mathrm{TLS}}$ is the estimate of C_{batt} based on dynamic data and $R_{\mathrm{TLS}}[\kappa]$ is the estimation error variance.

By following the same procedure, one can obtain the OCV based capacity estimates $C_{\mathrm{TO}}[\kappa]$ and the corresponding estimation error covariance $R_{\mathrm{TO}}[\kappa]$.

Now, let us assume the battery capacity to be a random variable that undergoes the following slowly changing Wiener process.

$$x_c[\kappa+1] = x_c[\kappa] + w_c[\kappa] \tag{51}$$

where $w_c[\kappa]$ is assumed to be zero mean white Gaussian noise with variance $Q_c[\kappa]$.

The capacity estimates $\widehat{C}_{\mathrm{TLS}}[\kappa]$ and $\widehat{C}_{\mathrm{TO}}[\kappa]$ fit the following observation model.

$$z_c[\kappa] = x_c[\kappa] + n_c[\kappa] \tag{52}$$

where

$$z_c\left[\kappa\right] \in \left\{\widehat{C}_{\mathrm{TLS}}\left[\kappa'\right], \widehat{C}_{\mathrm{TO}}\left[\kappa''\right]\right\} \tag{53}$$

κ' and κ'' are the time indices of latest estimates from the corresponding algorithms (TLS and TO, respectively), and $n_c[\kappa]$ is assumed to be a zero mean white noise with variance.

Table 2
Possible rest pairs for OCV based capacity estimation.

First rest (k)	Second rest ($k+N$)
1	t_2
t_1	t_3
t_1	t_4
t_2	t_3
t_2	t_4
t_3	t_4

Table 3
Computational complexity of the capacity estimation.

Method	Complexity
BFG based online capacity estimation - RLS (computation of (25))	$\mathcal{O}(L_c)$
BFG based online capacity estimation - TLS (computation of (29))	$\mathcal{O}(L_c)$
OCV based online capacity estimation	$\mathcal{O}(L_{\mathrm{c,ocv}})$
Fusion (computation of (56) and (57))	constant
Total complexity	$\mathcal{O}(L_c)$

$$R_c\left[\kappa\right] = \begin{cases} R_{\mathrm{TLS}}[\kappa] & \text{if } z_c\left[\kappa\right] = \widehat{C}_{\mathrm{TLS}}\left[\kappa\right] \\ R_{\mathrm{TO}}[\kappa] & \text{if } z_c\left[\kappa\right] = \widehat{C}_{\mathrm{TO}}\left[\kappa\right] \end{cases} \tag{55}$$

Now, whenever a new measurement $z_c[\kappa] \in \{\widehat{C}_{\mathrm{TLS}}[\kappa'], \widehat{C}_{\mathrm{TO}}[\kappa'']\}$ is received, where either $\kappa' = \kappa$ or $\kappa'' = \kappa$, the fused capacity estimate is obtained as.

$$\widehat{x}_c\left[\kappa\middle|\kappa\right] = \widehat{x}_c\left[\kappa-1\middle|\kappa-1\right] + \frac{P_c[k-1|k-1] + Q_c[\kappa-1]}{P_c[\kappa-1|\kappa-1] + Q_c[\kappa-1] + R_c[\kappa]} \times \left(z_c[\kappa] - \widehat{x}_c[k-1|k-1]\right) \tag{56}$$

where $\widehat{x}_c[\kappa-1|\kappa-1]$ is the previous update of capacity estimate and $P_c[\kappa-1|\kappa-1]$ is the previous estimation error variance which is updated as

$$P_c\left[\kappa\middle|\kappa\right] = \frac{R_c[\kappa]\left(P_c[\kappa-1|\kappa-1] + Q_c[\kappa-1]\right)}{P_c[\kappa-1|\kappa-1] + Q_c[\kappa-1] + R_c[\kappa]} \tag{57}$$

The above fusion approach can be similarly used for fusing RLS based capacity estimates.

2.5. Computational complexity

In this section, we discuss the complexity involved in estimating the battery capacity. Once the pairs of vectors $\mathbf{d}^k_s$ and $\mathbf{d}^k_c$ are given the BFG based online capacity estimates are obtained by computing (25) and (29) for RLS and TLS, respectively. The complexity of computing the SOC values $\mathbf{d}^k_s$ is referred to the SOC tracking block [6] and $\mathbf{d}^k_s$ can be computed through L_c additions. The complexity of computing (25) and (29) is linear in Ref. L_c; The lengths of the vectors $\mathbf{d}^k_{\mathrm{s,icv}}$ and $\mathbf{d}^k_{\mathrm{c,icv}}$ depend on the number of rest points a battery gets during a cycle and usually $L_{\mathrm{c,ocv}} \ll L_c$. Table 3 summarizes the required computational complexity for capacity estimation.

3. Simulation results

In this section, we provide performance analysis of the proposed capacity estimation method. First, we assess its performance using simulated battery data. Then, we use real usage data collected through hardware in the loop (HIL) experiments for performance assessment.

3.1. Performance analysis of BFG-based online capacity estimation method using simulated data

In this section we evaluate the performance of the BFG-based online capacity estimation methods using simulated data. We simulate typical battery usage data by following the details provided in Ref. [5]: First, typical battery usage profile, consisting of dynamic discharge and charging of the battery, was simulated in

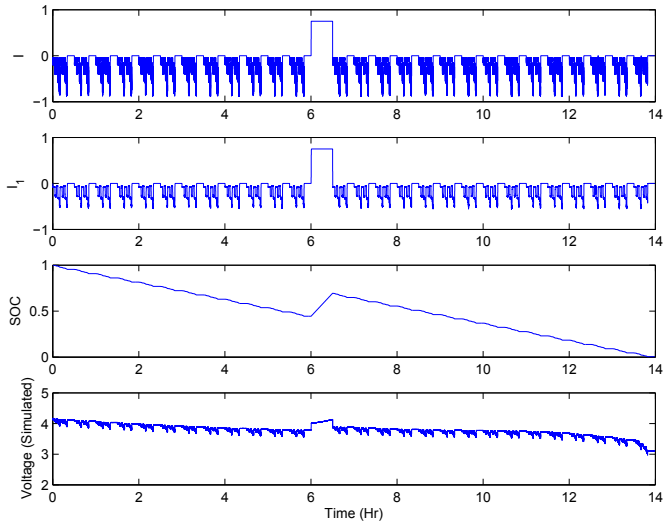

Fig. 5. Simulated data: Details. From top to bottom: Simulated load profile $i[k]$, computed current $x_1[k]$ through R_1, true SOC $x_s[k]$ and noisy battery terminal voltage $z_v[k]$.

terms of true load current $i[k]$. Then, measured current was simulated based on (3) by adding random noise with s.d. $\sigma_i = 10^{-3}$ A. Finally, the battery terminal voltage was computed according to battery equivalent Model 3 discussed in Ref. [5] assuming a voltage measurement error s.d. of $\sigma_v = 10^{-3}$ V and that the true initial SOC of the battery is $x_s[0] = 1$. It is assumed that $C_{\text{batt}} = 1.5$ Ah, $\eta_c = 0.998$, and $\eta_d = 1$ during the simulation. We use the same OCV parameter values and dynamic equivalent model parameter values as in Ref. [5] for the simulation.

In Fig. 5, we show the simulated battery usage data. The simulated load current $z_i[k]$ is shown in the top plot and the simulated voltage $z_v[k]$ is shown in the middle plot. The true SOC is computed based on Coulomb counting (2) by assuming the knowledge of the noiseless current profile $i[k]$ and true capacity and is shown in the plot at the bottom.

The simulated voltage $z_v[k]$ and current information $z_i[k]$ are fed to the battery fuel gauge presented in Ref. [6] which uses the method proposed in this paper for capacity estimation and our proposed approach in Ref. [5] for parameter estimation for adaptive SOC tracking. The SOC tracking algorithm uses $L_b = 200$ (20 s of data) for parameter estimation and $L_c = 30$ for capacity estimation.

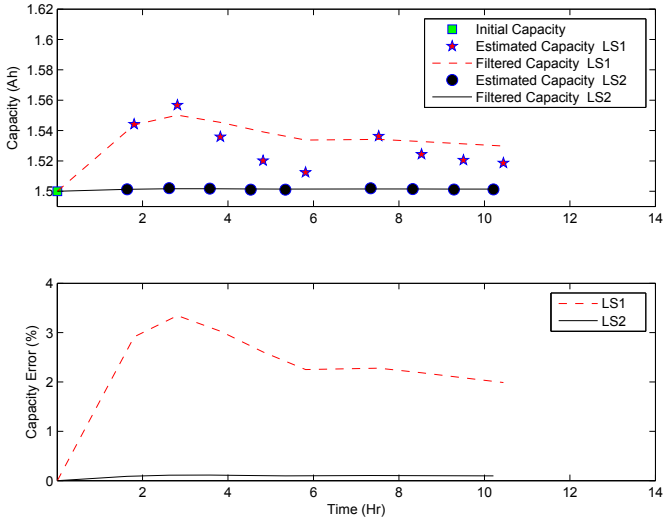

Fig. 6. Simulated data: Performance comparison of capacity estimation. Top plot shows the "Estimated Capacity" $C_{\text{TLS}}[k]$ against time. The bottom figure shows the percentage error in capacity estimation, $\epsilon_{C_{\text{batt}}}[k]$.

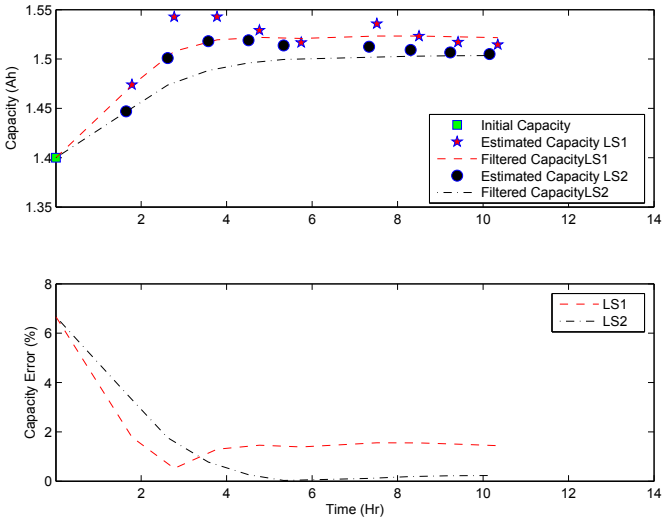

Fig. 7. Simulated data: Capacity estimation performance when the algorithm is initialized with the wrong capacity. The algorithm is given an initial capacity of 1.4 Ah whereas the true battery capacity is 1.5 Ah.

Next, we consider the performance of the algorithm in terms of battery capacity estimation by defining the capacity estimation error as

$$\epsilon_{C_{\text{batt}}}[k] = \frac{100}{C_{\text{batt}}}\sqrt{\frac{1}{M}\sum_{m=1}^{M}\left(C_{\text{batt}} - \widehat{C}_{\text{batt}}[k]\right)^2} \tag{58}$$

where C_{batt}(=1.5 Ah in this case) is the true value of the battery capacity and $\widehat{C}_{\text{batt}}[k]$ is the latest estimated battery capacity $\widehat{x}_c[\kappa|\kappa]$ at time k of the m^{th} Monte-Carlo run.

Fig. 6 shows the performance of BFG in terms of capacity estimation. The input to the capacity estimate, $\widehat{C}_{\text{TLS}}[\kappa]$, is denoted as "Estimated Capacity". The estimated capacity (both BFG and OCV based) is sent to the fusion algorithm. Since there are no rest

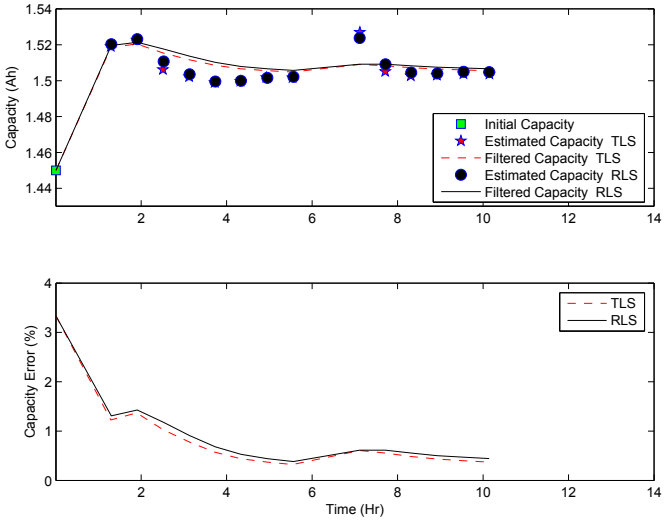

Fig. 8. Simulated data: Comparison of RLS and TLS methods for capacity estimation. Both methods use LS2 method for parameter estimation.

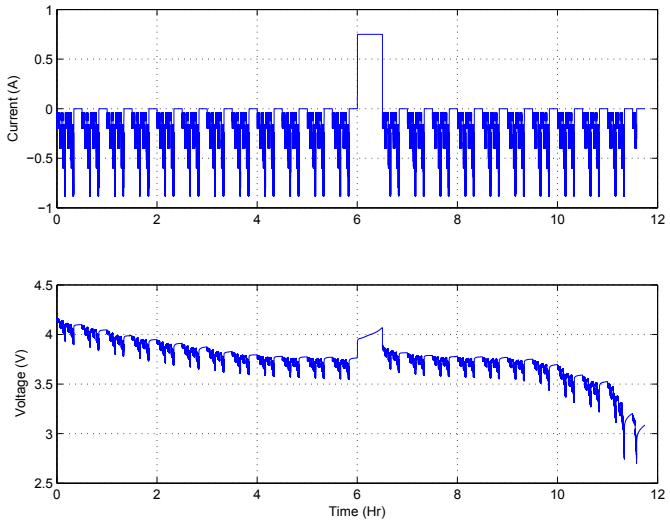

Fig. 9. HIL data: Details Top plot shows the terminal voltage of the battery and the second plot shows the load current. The battery model is Samsung AB463651 and the test temperature is 25°C.

periods in the data, all the capacity estimates are BFG based, hence the outputs from the fusion algorithm is labeled as "filtered capacity" instead of "fused capacity"; fused capacities are shown in Section 3.3. It must be noted that $\widehat{x}_C[\kappa|\kappa]$ is updated whenever there is a new capacity measurement. The output of fusing the capacity estimates $\widehat{x}_C[\kappa|\kappa]$, which is used by the BFG for SOC tracking, is shown as solid line. In other words, the solid line at any give time corresponds to C_{batt} used by the SOC tracking algorithm. In this example, the algorithm was given the knowledge of true capacity for initialization. In the next example, we demonstrate the performance with a wrong capacity initialization. The error in battery capacity estimation, $\boldsymbol{\epsilon}_{C_{\text{batt}}}[k]$ is plotted in the bottom of Fig. 6.

In Fig. 7, we show the ability of the algorithm to "catch up" if the true initial capacity is not known. This is particularly useful in practical applications where the same types of batteries will vary in their capacities.

In Fig. 8 we compare the performance of RLS and TLS methods for capacity estimation. This figure shows that the TLS method of capacity estimation is better than the RLS method. However, both

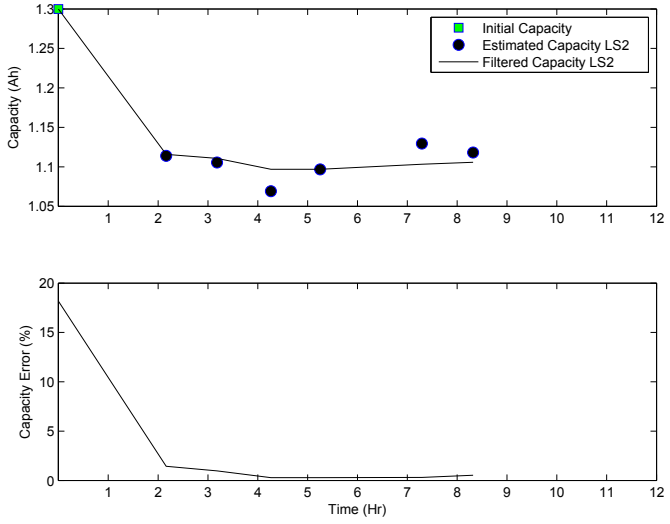

Fig. 10. HIL data: Battery capacity estimation. The true battery capacity was measured by a slow discharge.

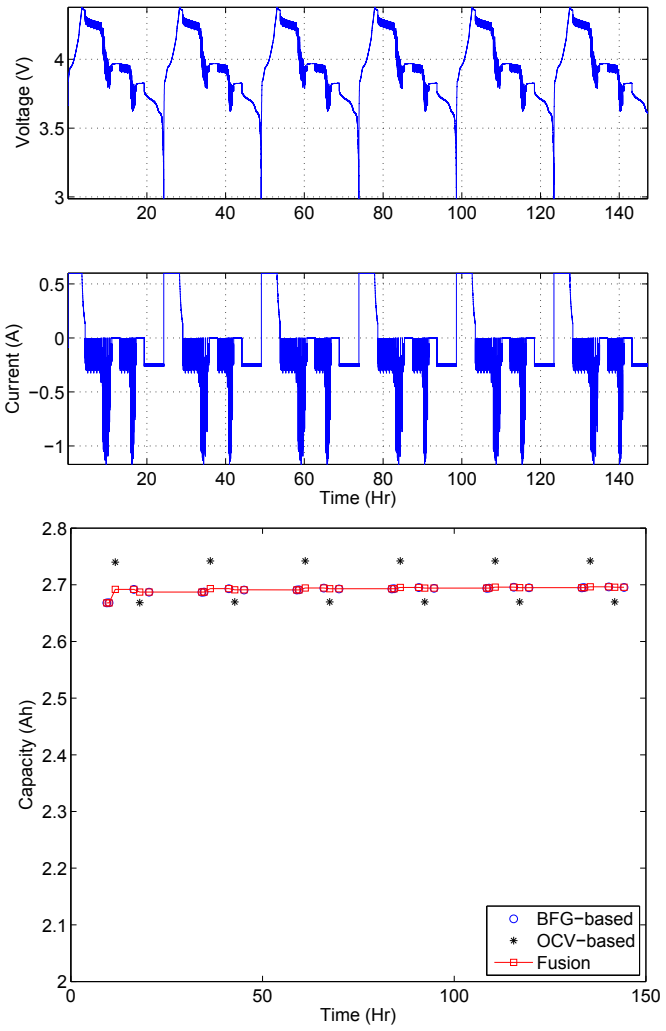

Fig. 11. Demonstration of capacity estimation through fusion of BFG and OCV based estimates. The top two plots show the measured voltage and current. The third plot shows the estimated capacities; the BFG based online capacity estimation is performed whenever there is dynamic current through the battery; the OCV based online capacity estimation is performed based on consequent battery resting periods. Whenever an online capacity estimate becomes available (either from BFG or OCV) it is used for Fusion.

methods provide capacity estimates that converge to within 1% accuracy in just one cycle of data.

The analysis on simulated data showed that the TLS estimate outperforms the RLS estimate of battery capacity. As a result, we will consider only the TLS estimate in the sequel for studying the performance analysis using real data.

3.2. Performance of BFG-based online capacity estimation method analysis using HIL data

In this section, the BFG based online capacity estimation algorithm is validated through experimental data collected from commercially available Li-ion battery cells. The BFG evaluation was also performed at a certain temperature using hardware-in-the-loop (HIL) test: a fully charged battery was placed inside a thermal chamber which was brought to the test temperature and then the battery was subjected to different charge–discharge current profiles and the battery terminal voltages were collected using a data acquisition system. In this paper, we limit our analysis to constant temperature evaluations only.

The SOC tracking algorithm developed in Ref. [5] was applied on the collected voltage and current data at each temperature. The OCV model parameters $\{K_i\}$ for these experiments were obtained offline by using a similar type of battery. Based on the configuration of the data acquisition system, the s.d. of the voltage measurement error was assumed as $\sigma_v = 10^{-3}$ V and the s.d. of the current measurement noise was assumed to be $\sigma_i = 10^{-3}$ A. The charging and discharging efficiencies were observed to be $\eta_c = 0.998$ and $\eta_d = 1$, respectively.

Fig. 9 shows the voltage and current data collected during HIL evaluations using a Samsung battery with serial number AB463651 at 25°C.

The performance of BFG in terms of battery capacity estimation is shown in Fig. 10. The true battery capacity is measured through a slow discharge test at the same temperature. The capacity estimation feature of the BFG is shown to be able to converge to the true capacity of the battery within 3–4 hours of operation.

3.3. Performance of capacity estimation through fusion analysis using HIL data

In this section, we demonstrate the capacity fusion method. The first two subplots of Fig. 11 show the data collected from a Samsung Galaxy (GS4) battery with serial number L1G6LLAGS. Starting with an empty battery, one full cycle of data was collected by first charging the battery until it becomes full and then applying dynamic loads separated by two rest periods. Then the battery is applied with a pulsed current of 240 mA average magnitude until the terminal voltage reaches 3 V. The same cycle of data is duplicated (not actually collected from the battery) in order to allow more rest points for the demonstration of the fusion algorithm. The outputs of the BFG based online capacity estimation method (TLS approach) and the OCV based online capacity estimation method are fused by the optimal fusion algorithm developed in Section 2.4.

The plot in the bottom of Fig. 11 shows the performance of the Fusion method. The BFG based online capacity estimates are available when there is dynamic load in the battery. The OCV based online capacity estimates are available whenever the battery becomes rested. Whenever there is a new estimate (either from the BFG method or OCV method), the Fusion routine is executed. It must be noted that the OCV based estimates are significantly different; the effect of hysteresis could be attributed to this. Since the same data is duplicated for several cycles, there is no change in the OCV based capacity estimates. In typical smart phone applications, a phone could be considered to be in rest while it "pings" the tower without any significant applications running for few minutes. Hence, there could be significantly more number of rest points within one cycle for OCV based capacity estimation. The objective here is to demonstrate the two types of capacity estimates and show the progression of the optimal Fusion algorithm.

4. Conclusions

This paper presented the following novel features for battery capacity estimation towards the advancement of battery fuel gauging:

(i) *A weighted recursive least squares (RLS) estimate of capacity with the derivation of exact weights.* We computed the exact formulation of the weights based on the SOC tracking error covariance and current measurement error standard deviation.

(ii) *A novel TLS approach for real time tracking of battery capacity.* The TLS estimate is derived in closed form and can be used for adaptive estimation by updating the covariance matrix with a fading memory.

(iii) *A novel method for adaptive capacity estimation based on OCV lookup of a rested battery.* We consider the source of OCV lookup error (hysteresis) in the derivations and propose an approach for adaptive estimation of capacity through OCV lookup.

(iv) *A robust approach for optimal fusion of capacity estimates obtained through different approaches.* Based on the capacity estimates and the estimation error covariances, the proposed approach uses a Kalman filter for adaptive, optimal fusion.

The applicability of the proposed approach can be discussed under four different scenarios:

1. *Applicability in the presence of temperature changes.* Both of the methods presented in this paper estimate the *total capacity* [7] of the battery. In Ref. [7] we define the total capacity as the maximum amount of Coulombs that can be discharged from a battery at cell temperature *T*. Typical capacity estimation takes from several minutes to a few hours during which the battery temperature is prone to change. The total capacity model (in terms of temperature) has to be included in the derivations for improved accuracy during temperature changes. We limit the focus of this paper to fixed temperature only.[3]
2. *Applicability in the presence battery aging.* Both methods of capacity estimation developed in this paper, BFG and OCV based, assume the *normalized OCV models* of [7]. The normalized OCV models are shown to be stable in the presence of aging.[4] Hence, the proposed capacity estimation procedure will perform well regardless of the age of the battery.
3. *Applicability for various battery chemistries.* The OCV model is the heart and soul of the online battery capacity estimation approach developed in this paper. When there are batteries of different chemistries to be gauged, there is an uncertainty in the OCV model. In Ref. [33], we develop a battery chemistry adaptive BFG where the BFG keeps a library of possible OCV model parameters and uses the probabilistic data association (PDA) algorithm [32] in order to associate the correct OCV model to the battery being gauged; we demonstrate the ability of the PDA algorithm to quickly find the correct OCV model. In summary, the proposed online capacity estimation methods in this paper will be effective when they are applied along with the battery chemistry adaptive BFG of [33].
4. *Applicability of the algorithm for varying dynamic load conditions.* Dynamic loading conditions affect both capacity estimation methods differently. Below, we provide brief details.
   - Effect of dynamic load variations on BFG based online capacity estimation: In Ref. [5], we discuss four possible ECMs as suitable for four different dynamic loading conditions of the battery. If a BFG uses a single ECM, the effect of different dynamic loading conditions might manifest as SOC estimation error due to model mismatch; this might affect the estimated capacity as well. However, it must be noted that the SOC

[3] It must be noted that the ECM parameters also vary with temperature. However, our voltage drop model based derivation in Ref. [5] requires only a few consecutive samples for ECM parameter estimation. Typically, we use 200 samples in Ref. [5] for parameter estimation; assuming a sampling interval of 100 ms, just 20 s of data is sufficient for accurate parameter estimation. The temperature change in Ref. 20 s can be neglected without compromising in accuracy.

[4] In Ref. [7], we report preliminary results that show that the OCV parameters obtained through normalized OCV modeling is unchanged over aging battery. The aging in Ref. [7] occurred through unused shelf life as well as repeated full-to-empty cycling using the same load profile. The effect due to other types of aging is currently being investigated.

estimation is performed at a *tiny* timescale (in milliseconds, see Table 1) whereas the capacity estimation is performed at a *medium* timescale (hours); which means that the effect of dynamic load variations will not be "felt" that much at the BFG based online capacity estimation as long as the model mismatch is temporary (In Ref. [5], we propose to use model 3, which suits the battery operations during major portions of the time).

- Effect of dynamic load variations on OCV based online capacity estimation: The hysteresis is a function of load current (among other factors such as temperature, SOC and the path); hence different dynamic loading conditions will result in different OCV lookup error values. The OCV based online capacity estimation approach was derived for this kind of situations; the adaptive estimation strategy is designed to mitigate the effect of hysteresis on capacity estimation.

Acknowledgments

The work reported in this paper was partially supported by NSF grants ECCS-0931956 (NSF CPS), ECCS-1001445 (NSF GOALI), CCF-1331850 (Cyber SEES), ARO grant W911NF-10-1-0369, and ONR grant N00014-10-1-0029. We thank NSF, ARO and ONR for their support of this work. Y. Bar-Shalom was partially supported by Grant ARO W911NF-10-1-0369. Any opinions expressed in this paper are solely those of the authors and do not represent those of the sponsors. The authors would like to thank Prof. Gregory L. Plett of University of Colorado at Colorado Springs for the collection of the HIL data. We thank the anonymous reviewers for providing useful comments and suggestions that resulted in the improved quality of this paper.

Appendix A. Derivation of capacity estimation error covariance

In this section, we derive the covariance of the differential error in (14). For convenience, the differential error (14) is rewritten below.

$$\tilde{w}_s[k] = \tilde{x}_s[k|k] - \tilde{x}_s[k+1|k+1] + w_s[k]$$

The objective is to compute the variance.

$$E\left\{\tilde{w}_s\left[k\right]\tilde{w}_s[k]^T\right\} \triangleq R_{\tilde{w}_s[k]} \tag{A.1}$$

Let us write the process equation (2) in the following forms:

$$x_s[k+1] = x_s[k] + c_h \Delta z_i[k] + w_s[k] \tag{A.2}$$

$$\hat{x}_s[k+1|k+1] = \hat{x}_s[k|k] + c_h \Delta z_i[k] + G[k+1]\nu[k+1] \tag{A.3}$$

where $\hat{x}_s[k+1|k+1]$ is the Kalman filter estimate of $x_s[k+1]$, $\nu[k+1]$ is the filter innovation and $G[k+1]$ is the Kalman gain.

The difference between (A.2) and (A.3) is

$$\tilde{x}_s[k+1] = \tilde{x}_s[k] + w_s[k] - G[k+1]\nu[k+1] \tag{A.4}$$

which can be rearranged to the following form

$$\tilde{x}_s[k] - \tilde{x}_s[k+1] + w_s[k] = \tilde{w}_s[k] = G[k+1]\nu[k+1] \tag{A.5}$$

Hence,

$$R_{\tilde{w}_s[k]} = G[k+1]^2 S\left[k+1\right] \tag{A.6}$$

where $S[k+1]$ is the innovation covariance.

Appendix B. Closed form derivation of TLS capacity estimate

Let us write the 2×2 matrix $\mathbf{A} \triangleq \mathbf{S}_{\mathbf{H}}^{\kappa}$ as

$$\mathbf{A} = \begin{bmatrix} \sigma_{11} & \sigma_{12} \\ \sigma_{12} & \sigma_{22} \end{bmatrix} \tag{B.1}$$

The eigenvalues of $\mathbf{A}$ can be written as

$$\lambda_1 = \frac{\sigma_{11} + \sigma_{22} + \sqrt{(\sigma_{11} - \sigma_{22})^2 + 4(\sigma_{12})^2}}{2} \tag{B.2}$$

$$\lambda_2 = \frac{\sigma_{11} + \sigma_{22} - \sqrt{(\sigma_{11} - \sigma_{22})^2 + 4(\sigma_{12})^2}}{2} \tag{B.3}$$

where λ_1 is the largest eigenvalue and λ_2 is the smallest eigenvalue.

The eigenvector corresponding to λ_2 is

$$\mathbf{v}_2^{\kappa} = \begin{bmatrix} \dfrac{-\sigma_{12}}{\sqrt{\sigma_{12}^2 + (\sigma_{11} - \lambda_2)^2}} \\ \dfrac{\sigma_{11} - \lambda_2}{\sqrt{\sigma_{12}^2 + (\sigma_{11} - \lambda_2)^2}} \end{bmatrix} \tag{B.4}$$

The estimated capacity now becomes

$$\begin{aligned} \widehat{C}_{\mathrm{TLS}}^{-1}\left[\kappa\right] &= -\frac{\mathbf{v}_2^{\kappa}(1)}{\mathbf{v}_2^{\kappa}(2)} \\ &= \frac{\mathbf{S}_{\mathbf{H}}^{\kappa}(1,2)}{\mathbf{S}_{\mathbf{H}}^{\kappa}(1,1) - \Lambda^{\kappa}(2,2)} \end{aligned} \tag{B.5}$$

Appendix C. Transformation of the inverse capacity estimates

In this appendix, we present an approach to get the capacity estimate and the estimation error variance based on the inverse estimate and the inverse estimation error variance. Our derivations are based on [34,35].

Let us assign simple variables for inverse capacity estimate and the error variance, i.e.,

$$x \triangleq C_{\mathrm{TLS}}^{-1}\left[\kappa\right] \tag{C.1}$$

$$x_0 \triangleq E\{x\} = \widehat{C}_{\mathrm{TLS}}^{-1}\left[\kappa\right] \tag{C.2}$$

$$R_x \triangleq E\left\{(x - x_0)^2\right\} = \widehat{R}_{\mathrm{TLS}}\left[\kappa\right] \tag{C.3}$$

Defining

$$y \triangleq f(x) = \frac{1}{x} \tag{C.4}$$

our objective is to find approximations for $E\{y\}$ and $E\{(y - E\{y\})^2\}$.

Appendix C.1. Expected value of y

The second order Taylor series approximation is given by

$$y = f(x) = f(x_0) + f'(x_0)(x - x_0) + \frac{1}{2}f''(x_0)(x - x_0)^2 \tag{C.5}$$

The second order approximation of $E\{y\}$ is given by

$$E\{y\} = E\{f(x_0)\} + f'(x_0)\underbrace{(E\{x\} - E\{x_0\})}_{=0} + \frac{1}{2}f''(x_0)E\left\{(x-x_0)^2\right\} = \frac{1}{x_0} + \frac{R_x}{x_0^3} \tag{C.6}$$

Appendix C.2. Variance of the expected value of y

Let us expand $f(x)$ as a first order Taylor series around the true value. x_0.

$$y = f(x) = f(x_0) + f'(x_0)(x - x_0) \tag{C.7}$$

The variance of y is given by

$$E\left\{(y - E\{y\})^2\right\} = E\left\{(f'(x_0)(x-x_0))^2\right\} = \frac{R_x}{x_0^4} \tag{C.8}$$

Now, the expected values of the capacity estimate and its estimation error variance are given by

$$C_{\mathrm{TLS}}[\kappa] = \frac{1}{\widehat{C}_{\mathrm{TLS}}^{-1}[\kappa]} + \frac{\widehat{R}_{\mathrm{TLS}}[\kappa]}{\left(\widehat{C}_{\mathrm{TLS}}^{-1}[\kappa]\right)^3} \tag{C.9}$$

$$R_{\mathrm{TLS}}[\kappa] = \frac{\widehat{R}_{\mathrm{TLS}}[\kappa]}{\left(\widehat{C}_{\mathrm{TLS}}^{-1}[\kappa]\right)^4} \tag{C.10}$$

References

[1] M. Einhorn, F.V. Conte, C. Kral, J. Fleig, IEEE Trans. Ind. Appl. 48 (2) (2012) 736–741.
[2] R. Xiong, F. Sun, X. Gong, C. Gao, Appl. Energy 113 (2014) 1421–1433.
[3] G.L. Plett, J. Power Sources 196 (4) (2011) 2319–2331.
[4] M.A. Roscher, O. Bohlen, J. Vetter, Int. J. Electrochem. 2011 (2011). Article ID 984320.
[5] B. Balasingam, G.V. Avvari, B. Pattipati, K.R. Pattipati, Y. Bar-Shalom, J. Power Sources (2014), http://dx.doi.org/10.1016/j.jpowsour.2014.07.034.
[6] B. Balasingam, G.V. Avvari, B. Pattipati, K.R. Pattipati, Y. Bar-Shalom, J. Power Sources (2014) under review.
[7] B. Pattipati, B. Balasingam, G.V. Avvari, K. Pattipati, Y. Bar-Shalom, J. Power Sources 269 (10 December 2014) 317–333.
[8] B. Balasingam, G.V. Avvari, B. Pattipati, K.R. Pattipati, Y. Bar-Shalom, J. Power Sources (2014) under review.
[9] S. Santhanagopalan, R.E. White, J. Power Sources 161 (2) (2006) 1346–1355.
[10] Y.-S. Lee, W.-Y. Wang, T.-Y. Kuo, IEEE T. Ind. Electron. 55 (1) (2008) 229–239.
[11] O. Gérard, J.-N. Patillon, F. d'Alché Buc, in: Artificial Neural NetworksI-CANN'97, Springer, 1997, pp. 1095–1100.
[12] M. Charkhgard, M. Farrokhi, IEEE T. Ind. Electron. 57 (12) (2010) 4178–4187.
[13] A. Millner, in: Innovative Technologies for an Efficient and Reliable Electricity Supply (CITRES), 2010 IEEE Conference on, IEEE, 2010, pp. 349–356.
[14] P. Ramadass, B. Haran, P.M. Gomadam, R. White, B.N. Popov, J. Electrochem. Soc. 151 (2) (2004) A196–A203.
[15] P. Ramadass, B. Haran, R. White, B.N. Popov, J. Power Sources 123 (2) (2003) 230–240.
[16] G. Ning, R.E. White, B.N. Popov, Electrochim. Acta. 51 (10) (2006) 2012–2022.
[17] S. Santhanagopalan, Q. Guo, P. Ramadass, R.E. White, J. Power Sources 156 (2) (2006) 620–628.
[18] A. Abdollahi, N. Raghunathan, B. Pattipati, X. Han, B. Balasingam, K.R. Pattipati, Y. Bar-Shalom, J. Power Sources (2014) under review.
[19] P. Rong, M. Pedram, IEEE Transactions 14 (5) (2006) 441–451.
[20] X. Lin, J. Park, L. Liu, Y. Lee, A. Sastry, W. Lu, J. Electrochem. Soc. 160 (10) (2013) A1701–A1710.
[21] G. Ning, B. Haran, B.N. Popov, J. Power Sources 117 (1) (2003) 160–169.
[22] J. Vetter, P. Novak, M. Wagner, C. Veit, K.-C. Möller, J. Besenhard, M. Winter, M. Wohlfahrt-Mehrens, C. Vogler, A. Hammouche, J. Power Sources 147 (1) (2005) 269–281.
[23] M. Broussely, P. Biensan, F. Bonhomme, P. Blanchard, S. Herreyre, K. Nechev, R. Staniewicz, J. Power Sources 146 (1) (2005) 90–96.
[24] M. Broussely, S. Herreyre, P. Biensan, P. Kasztejna, K. Nechev, R. Staniewicz, J. Power Sources 97 (2001) 13–21.
[25] G. Sarre, P. Blanchard, M. Broussely, J. Power Sources 127 (1) (2004) 65–71.
[26] H. He, X. Zhang, R. Xiong, Y. Xu, H. Guo, Energy 39 (1) (2012) 310–318.
[27] Y.-H. Chiang, W.-Y. Sean, J.-C. Ke, J. Power Sources 196 (8) (2011) 3921–3932.
[28] Y. Bar-Shalom, X.R. Li, T. Kirubarajan, Estimation with Applications to Tracking and Navigation: Theory Algorithms and Software, John Wiley & Sons, 2004.
[29] I. Markovsky, S. Van Huffel, Signal Process 87 (10) (2007) 2283–2302.
[30] L. Crassidis, Y. Cheng, Error-covariance Analysis of the Total Least Square Problem, American Institute of Aeronautics and Astronautics.
[31] R. Hamming, Numerical Methods for Scientists and Engineers, Courier Dover Publications, 2012.
[32] Y. Bar-Shalom, P. K. Willett, X. Tian, Tracking and Data Fusion, A Handbook of Algorithms. (Yaakov Bar-Shalom).
[33] G.V. Avvari, B. Balasingam, K. Pattipati, Y. Bar-Shalom, J. Power Sources (2014) under review.
[34] R.C. Elandt-Johnson, N.L. Johnson, Survival Models and Data Analysis, Wiley, New York, 1980.
[35] A. Stuart, J. K. Ord, Kendalls Advanced Theory of Statistics (volume 1), Arnold: London.